Received: 24 August 2024 | Revised: 26 September 2024 | Accepted: 1 October 2024

DOI: 10.1002/htj.23208

ORIGINAL ARTICLE

HEAT TRANSFER WILEY

Performance enhancement for a novel cylindrical system Li-ion battery with MXene-based dielectric fluid for immersion cooling

Nilesh Krishnadhari Singh | **Rashmi Rekha Sahoo**

Department of Mechanical Engineering, IIT (BHU), Varanasi, Uttar Pradesh, India

Correspondence
Rashmi Rekha Sahoo, Department of Mechanical Engineering, IIT (BHU), Varanasi-221005, UP, India.
Email: rrsahoo.mec@itbhu.ac.in

Abstract

This research looks at the impact of dielectric fluids and fluid speeds on cell temperature control in innovative cylindrical lithium-ion batteries during high-rate discharges (C-rate) using the multiscale multidomain battery model. The goal is to improve the battery thermal management system to increase battery performance, longevity, and safety. The present study includes reducing thermal strains, enhancing efficacy, and forestalling overheating risks across various applications in electrified systems. The assessment focuses on four dielectric fluids—ester, mineral, kerosene, and Novec 7200—flowing at 0.01 m/s to gauge their efficiency in managing cell temperatures. Results demonstrate the criticality of effective thermal management in maintaining optimal battery performance and longevity. Ester oil emerges as the most efficient coolant, maintaining cell temperatures at 305.84 K and showcasing a 44% reduction compared with scenarios without coolant. In contrast, kerosene oil, mineral oil, and Novec 7200 yield temperature reductions of 42.86%, 42.51%, and 43.11%, respectively.

Abbreviations: BMS, battery management system; BTMS, battery thermal management system; CFD, computational fluid dynamics; C-rate, charge/discharge rate; ECM, equivalent circuit model; EV, electric vehicle; FFIC, forced flow immersion cooling; HEV, heavy electrical vehicle; LIB, lithium-ion battery; NTGK, Newman, Tiedemann, Gu, and Kim; OCV, open circuit voltage; PCM, phase-change material; SOC, state of charge.

Furthermore, combining 1% v/v. MXene nanoparticles with ester oil enhance cooling capabilities, with remarkable cell temperature reductions of 50% at 0.01 m/s velocity. Subsequent increments in flow velocity lead to enhanced cooling effects: at 0.05 and 0.1 m/s, reductions reach 51.89% and 52.155%, escalating to 52.58% and 54% at 0.5 and 1.0 m/s, correspondingly.

KEYWORDS

C-rate MXene nanoparticles, dielectric fluid, immersion cooling, NTGK modeling

1 | INTRODUCTION

Efficient thermal management in batteries is critical for performance and safety. Advanced thermal control strategies are essential for optimizing battery operation, enhancing longevity, and preventing thermal runaway risks. Immersion cooling battery thermal management systems (BTMSs) utilize a submerged approach to control the batteries' temperature in electric vehicles (EVs) or stationary energy storage systems. In this method, batteries are immersed in a liquid with thermal conductivity, like, dielectric fluid or coolant, which efficiently dissipates heat generated during operation. The fluid extracts heat from the battery cells, maintaining optimal operating temperatures to enhance performance, longevity, and safety. Immersion cooling ensures uniform heat distribution, mitigating thermal hotspots and potential thermal runaway events. This technology offers superior thermal management to traditional air or liquid cooling (LC) systems, optimizing battery efficiency and reliability. A research review by Wu et al.[1] highlights the developments in EVs by describing temperature-sensitive battery performance issues, emphasizing battery modeling liquid thermal management systems, and suggesting integrated vehicle thermal management for improved efficiency and energy optimization. Fayaz et al.[2] reviewed the paper covering temperature factors and important structural design concerns, emphasizing improving thermal and structural design parameters for Li-ion batteries (LIBs) in various BTMSs. The study by Wang et al.[3] examined the thermal behavior of LIBs in electric powertrains and highlights how crucial battery thermal management is to achieving peak efficiency. It covers thermal models, management techniques, difficulties, and the requirement for better BTM technologies to increase battery safety and longevity. In their assessment of LIB technologies, Kumar and Goel[4] emphasize how crucial efficient battery heat management is to achieving peak performance. Heat pipe systems are highlighted, along with a comparison of temperature metrics and a discussion of material modifications for increased efficiency. The significance of battery thermal management for LIBs in EVs is covered in the study by Kim et al.,[5] which reviews existing systems, classifies them according to thermal cycles, and suggests a unique approach to improve temperature control and battery performance. The study by Wang et al.[6] presented a novel way to improve the BTMS that uses air cooling by employing a parallel plate installation methodology. Simulations conducted on nine different BTMS configurations demonstrate notable gains in cooling efficiency and a decrease in the system's maximum temperature and temperature differential. By improving the flow patterns, Chen et al.[7] improved the cooling performance of air-cooled BTMSs. Asymmetrical BTMS demonstrates high efficiency with an inlet/outlet in the middle through numerical analysis and experimental confirmation. With a 12% reduction in power usage, optimization further lowers the maximum temperature by 4.5 K and the cell temperature difference by 7.7 K. A unique BTMS model with additional vents and reciprocating airflow is introduced in the Wang et al.[8] study. A 50.2% reduction in temperature differential and a temperature drop of 4.0 K are the results of optimization. Moreover, adding variable vents improves temperature uniformity by lowering the maximum temperature by 4.12–3.24 K and the maximum temperature difference by 1.55–1.24 K. A parallel air-cooled system with a control method for battery pack cooling is introduced in the paper of Chen et al.[9] The temperature differential between the cells is significantly reduced by over 67%, regulated below 0.5 K following flow-type transitions, improving thermal management efficiency in various circumstances. Akbarzadeh et al.[10] used computational fluid dynamics (CFD) simulations to compare liquid and air thermal management systems for a LIB module. The liquid-cooled system exhibits greater thermal performance with an average temperature in the hottest cell around 3°C lower for 0.5 W power usage. A composite thermal management system integrating mini-channel LC and air cooling is suggested for cylindrical LIBs by Yang et al.[11] The findings show that with a maximum temperature reduction of 304.98 K, a suitable tube spacing, flow direction, and spacer combination may maintain a temperature difference within 4.13 K at a water inlet flow rate of 0.0003 kg/s. At 80% depth of discharge (*DoD*), the maximum temperature and temperature differential decrease by 2.22 and 2.04 K, respectively, with additional air cooling at 4 m/s. With automatic fan control, the temperature differential can be further controlled within 5.0 K. The study by Chen et al.[12] optimized cell spacings using CFD and an iterative approach, resulting in improved performance for the parallel air-cooled BTMS. The findings indicate a decrease in both the maximum pack temperature and the cell temperature differential, resulting in enhanced cooling effectiveness without rising power consumption at different airflow rates. Wang et al.[13] presented a novel modular liquid-cooled battery system and investigate the effects of cooling modes and coolant flow rates on thermal behavior. The results show the significance of flow rate and parallel cooling for effective cooling. For battery thermal management, a novel method combining liquid cooling tubes (LCTs) and static immersion cooling is presented in the paper by Zou et al.[14] At 25°C ambient, the maximum temperature is less than 43.3°C, and the temperature differential is less than 2.62°C when 10 LCTs are used at 0.2 m/s intake velocity. With a temperature differential of less than 3.51°C at 40°C ambient, the temperature stays below 55.72°C, demonstrating similar cooling effectiveness without additional fluid circulation systems. In a study by Satyanarayana et al.,[15] forced air cooling, mineral oil cooling, and thermomineral oil cooling are contrasted on a stack of 10 Ah LIBs. The following results demonstrate the significant temperature drops at a 3C discharge rate: 43.83% with forced air cooling, 49.17% with terminal oil cooling, and 51.54% with mineral oil cooling. The efficiency of various dielectric fluids in direct LC of LIBs is assessed by Jithin and Rajesh,[16] which achieves temperature rises below 5°C at 2C discharging with higher mass flow rates. Compared with mineral oil and deionized water, engineered fluids perform better and use less energy. In a study by Hemavathi et al.,[17] forced flow immersion cooling (FFIC) based on single-phase synthetic ester oil optimizes the thermal performance of LIB packs. Compared with air convection and static flow immersion cooling, FFIC reduces temperature rise by 51% and 35%, respectively, at a flow rate of 5 L/min and a pressure drop of 228.44 Pa. Qi et al.[18] introduced a thermal management system for a Swiss roll-type battery, optimizing structural parameters, coolant flow rate, type, and temperature. After optimization, the Swiss roll battery module exhibits a maximum temperature of 300.4 K, a temperature difference of 3.3 K, and a cooling belt height of 55 mm, reducing values by 4 K, 0.2 K, and 10 mm, respectively, compared with the reference group. A triple tube heat exchanger using MXene nanofluids showed a 12.51%

increase in heat transfer coefficient over Al_2O_3 nanofluids and a 20% increase over water, according to a study by Gaur et al.[19] In their LIB thermal regulation study, Kumari and Paswan[20] compared cooling by air, water, and graphene–water nanofluid. Greater cooling efficiency is demonstrated using nanofluid, whose maximum temperature is lowered to 300.656 K. Somasundaram et al.[21] studied the two-dimensional transient mathematical model developed for the passive thermal management of LIBs to facilitate in-depth analysis and optimization. This model considers heat generation, temperature-dependent properties, and phase-change material (PCM) cooling effects. According to a study by Zhang et al.,[22] effective thermal management is necessary to prevent thermal safety problems like thermal runaway in EVs using power LIBs. PCM-based cooling exhibits potential because of its high heat capacity; nonetheless, its low thermal conductivity makes it impractical and necessitates improved methods for EV integration. A thermal management module that combined PCM (CPCM) with a copper pipe and LC demonstrated enhanced heat dissipation, especially at high temperatures. Integrating a dynamic liquid cooling (DLC) mode reduced energy consumption by operating LC intermittently, with LC activation time affecting cooling behavior. A thermal management module that CPCM with a copper pipe and LC demonstrated enhanced heat dissipation, especially at high temperatures. Integrating a DLC mode reduced energy consumption by operating LC intermittently, with LC activation time affecting cooling behavior. Weng et al.[23] examined tubular PCMs under varying liquid temperatures to model battery module conditions. In their study, Luo et al.[24] evaluate the designs of Battery-PCM and Battery-PCM-Fins at discharge rates of 3C and 5C and ambient temperatures of 25°C and 40°C. Of the five LC plate configurations, Design IV is shown to be the most efficient. To improve heat transfer in hybrid electric vehicle and EV, Shojaeefard et al.[25] evaluate six configurations of a BTMS using PCMs with different fin alignments, emphasizing the superior cooling effect of systems with horizontal fins. Pu et al.[26] showed that the new hybrid BTMS for LIBs, which combines PCM and LC, has a superior design. It lowers system mass and battery temperature while improving performance metrics. The experimental investigation by Chen et al.[27] on the power capabilities of LIBs under various conditions helps provide accurate SOP estimation for EV battery management systems. An analysis by Tran et al.[28] revealed that 1RC with hysteresis worked best for lithium iron phosphate and lithium nickel cobalt aluminum oxide LIB models, whereas 1RC was ideal for lithium nickel manganese cobalt oxide and lithium manganese oxide LIB models, highlighting the influence of chemistries on equivalent circuit model selection. Using RT-47 PCM and NePCM with Al_2O_3 nanoparticles, Bais et al.[29] experimental study on a novel BTMS revealed better thermal performance and lighter LIBs drained at 3C. Fly ash is investigated by Nagaraja et al.[30] as an inoculant in aluminum AA 5083/7.5 SiC composites to improve tensile and impact strengths up to 2 wt%, supporting the material's properties and aiding in grain refinement. Microstructural and analytical data are used to support this claim. Using CFD models, Panchal[31] improves cylindrical battery cooling in EVs and highlight the effects of temperature, air velocity, and cell spacing on uniform heat dissipation and system performance. Pu et al.[32] research on a novel Variable Cross-Section Double serpentine-channel cold plate enhances the performance of LIBs at high discharge rates by lowering temperatures and pressure loss. By prolonging trigger points and lowering peak temperatures, Talele et al.[33] used graphene-enhanced composite phase transition material substantially delay the onset of thermal runaway in LIBs, hence improving safety. Thermal runaway modeling in LIBs, including triggering variables, heat generation, and gas venting, is examined by Jiaqiang et al.[34] This modeling helps build safer battery systems and mitigate hazards more efficiently. The use of composite PCM with LC in Xiao et al.[35] study improves battery safety by postponing the spread of thermal runaway, which is affected by variables, such as coolant flow rate, battery spacing, CPCM thermal conductivity, and cooling plate channel number. A 10% EG CPCM was suggested in Shengxin et al.[36] research on ternary polymer LIBs for better heat dissipation and thermal safety during 3C discharge in hot climates. According to research by Liu et al.,[37] a composite cooling method that combines air cooling with PCM greatly increases heat dissipation in LIB packs in hot regions, improving both performance and safety. To achieve quick preheating at low temperatures, Jiaqiang et al.[38] investigated the designs and optimizations of a preheating system for large-capacity lithium batteries employing heating film and PCM. According to Ma et al.[39] research, a unique composite PCM with a metal–organic framework is proposed for effective battery thermal management. This material enhances thermal characteristics and stabilizes battery temperatures.[40] Synthesis of LA/EG@HPC, composite PCM, enhances battery thermal management by providing efficient heat transfer and reducing cell temperatures during operation. A novel hierarchical porous CNT/MOF-199 composite PCM is presented by Ma et al.[41]; it improves thermal insulation performance in LIBs at low temperatures and exhibits increased latent heat (97.1 J/g). Nitrogen-doped hierarchical porous carbon composite with stearic acid has improved thermal characteristics, improving battery thermal optimization by 7.89% at −20°C. This is according to a study by Ma et al.[42] Yi et al.[43] studied the composite cooling system utilizing PCM and LC was modified. The results demonstrated improved performance with changes to expanded graphite, spacing, and flow rate for effective thermal management.

This research paper presents a novel investigation into the cooling performance of novel cylindrical shell LIB packages under high discharge conditions, specifically focusing on using different dielectric fluids enhanced with MXene nanoparticles. Prior studies have predominantly focused on active cooling systems; however, this work explores passive cooling strategies, addressing a significant gap in the literature regarding integrating MXene nanoparticle-enhanced dielectric fluids at varying velocities. The study uses numerical methods to evaluate the thermal dynamics of ester oil, kerosene oil, mineral oil, Novec 7200, and 1% v/v—MXene nanoparticles-based ester as they pass through battery modules. The comprehensive analysis includes assessments of cell temperature, fluid temperature, and voltage drop under 5C-rate discharges. Additionally, the research delineates the thermal contours of both standard and nanoenhanced dielectric oils within the battery system, providing insights into the effectiveness of these cooling strategies for managing heat in LIBs under extreme operational stresses. This exploration contributes a critical perspective to the design of efficient thermal management systems for high-performance battery applications.

2 | MATHEMATICAL MODELING

2.1 | Geometrical specification

Battery pack design is critical to modern technology, especially in EVs, portable electronics, and renewable energy storage systems. The block diagram described a series-connected battery pack consisting of two cylindrical cells connected by busbars, cathodes, and anodes. Each cell is 65 mm long and 18 mm in diameter, while the connecting components are all 18 mm in diameter and 5 mm long. The entire assembly is encased in a dielectric fluid layer, 3 mm thick, providing electrical insulation and thermal management. This configuration underscores the significance of precise component sizing and fluid dynamics in ensuring optimal performance and safety of the battery pack. The length of the connecting components influences their electrical resistance and mechanical stability. Shorter lengths reduce electrical resistance by minimizing the path length for current flow, improving electrical efficiency.

Moreover, shorter lengths enhance mechanical stability by reducing the leverage exerted on the connections, mitigating the risk of mechanical failure under stress. Effective thermal management is crucial for maintaining the optimal operating temperature range of the battery cells, as excessive heat can degrade performance, reduce cycle life, and pose safety hazards, such as thermal runaway. By encasing the assembly in a dielectric fluid layer shown in Figure 1, heat generated during operation can be efficiently dissipated to the surrounding environment through conduction and convection, thereby preventing overheating and ensuring long-term reliability.

The block diagram, Figure 1, illustrates a series-connected battery pack with carefully selected component dimensions and fluid dynamics to optimize performance and safety. The dimensions of the cylindrical cells, connecting components, and dielectric fluid layer are chosen based on energy density, electrical efficiency, mechanical stability, and thermal management considerations. By meticulously designing each component and considering their interactions, engineers can create battery packs that meet the demanding requirements of modern technology while ensuring reliability and safety in various applications. Table 1[15–18,44] provides comprehensive parameters for the entire battery pack, whereas Table 2[15–19] presents the thermophysical properties of dielectric fluids.

2.2 | Meshing

The meshing process involves creating a grid-like structure over the surface of the battery pack to simulate various physical phenomena accurately. A specific mesh configuration is structured to optimize accuracy and computational efficiency for the CFD simulation in ANSYS Fluent. The preferred mesh type is designed with linear elements due to their adequate balance between simplicity and precision. An element size of 1 mm is chosen as the base size for the mesh, with a maximum size set at 2.0 mm. This ensures that the mesh is fine enough to capture

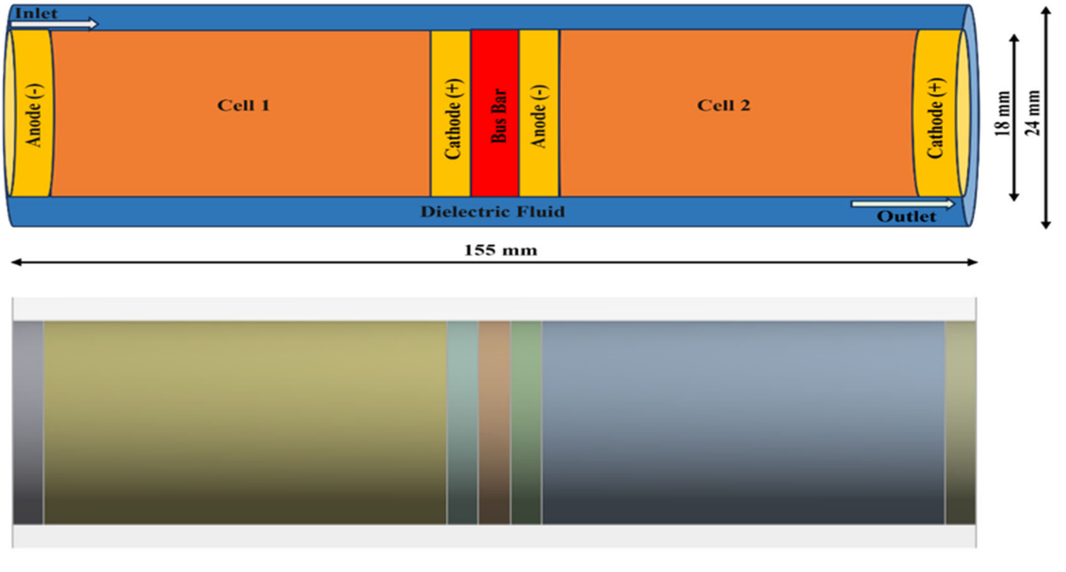

FIGURE 1 Specifications of the submerged cylindrical battery pack (three-dimensional and actual view).

TABLE 1 Battery material's thermophysical characteristics.[15–18,44]

Parameter	Value
Cell density/active zone material (kg/m^3)	2092
Busbar density (kg/m^3)	8978
Air density in kilograms per cubic meter	1.225
Busbar thermal conductivity (W/m K)	387.6
Aluminum thermal conductivity (W/m K)	202.4
Cathode/anode material	Copper
Copper density	8978
Copper specific heat (J/kg K)	381
Copper thermal conductivity (W/m K)	387.6
Cell's nominal capacity (in Ah)	4.2
Cell's nominal voltage (in volts)	4
Maximum voltage at which to switch off (V)	4.3
Volts for the minimum cut-off voltage	3
Electrolyte material	Active zone material
Active zone material specific heat (J/kg K)	678
Active zone material thermal conductivity (W/m K)	18.2
The cell's length (mm)	65
The cell's diameter (mm)	18

necessary details yet coarse enough to limit computational demand. The maximum element quality is 0.9989, and the maximum skewness of mesh is 0.5612.

Mesh defeaturing is enabled with a size of 0.005 mm. This feature is crucial for eliminating small geometric features that do not significantly impact the overall simulation results, thereby reducing unnecessary computational load without sacrificing the fidelity of essential details. The mesh configuration also incorporates curvature capture, setting the curvature minimum size at 0.01 mm. This attribute is significant as it allows the mesh to accurately model the geometry wherever there are curves, enhancing the precision of flow dynamics around these features. The curvature normal angle is set to its default value of 18°, facilitating a balanced approach between capturing curved surfaces and optimizing mesh element distribution. The growth rate is established at 1.2, controlling how mesh size increments from finer regions near geometric details to coarser regions away from these areas. A moderate growth rate typically helps ensure a smooth transition, enhancing solution stability and accuracy. The mesh settings do not include adaptive sizing, meaning the specified parameters are uniformly applied throughout the meshing process to maintain consistency. As shown in Figure 2, this deliberate mesh configuration provides a well-tailored framework suitable for resolving the complex flow behaviors and thermal patterns within the battery module for efficient CFD analysis using Fluent.

TABLE 2 Dielectric fluid and nanoparticle properties.[15–19]

Fluid parameter	Mineral oil	Kerosene oil	Novec 7200	Ester oil	Ester oil + MXene	MXene nanoparticle
Density (kg/m^3)	924	785	1420	961	1028	3190
Specific heat capacity (J/kg K)	1900	2100	1220	1919	2090	3760
Thermal conductivity (W/m K)	0.13	0.145	0.068	0.147	0.1605	55.8
Dynamic viscosity (m^2/s)	0.052	0.00192	0.00069	0.041	0.04424	–

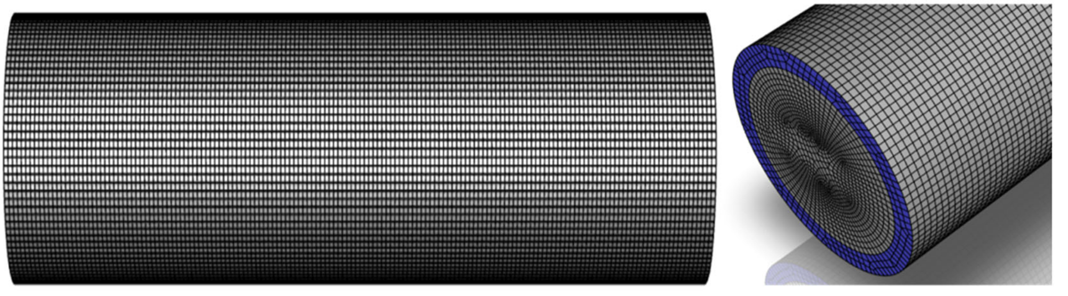

FIGURE 2 Design a submerged cylindrical battery pack with a modular three-dimensional topology.

TABLE 3 The battery pack's cylindrical mesh matrix.

Parameter	Value
Number of nodes	274,818
Number of elements	297,680
Elemental quality	0.99889
Skewness	0.56512

Presented in Table 3 is the mesh matrix detailing the distribution and arrangement of elements within the battery pack model. Through Figure 2, the results of a mesh have been checked and revealed a trend where increasing the number of cells leads to a decrease in cell temperature, showcasing the mesh's influence on the simulation outcomes.

Subsequently, Figure 3 demonstrates a marginal change of only 0.35% in cell temperature when the cell count is increased from 100,000 to 350,000, as presented in Figure 3. Thus, after thorough investigation and analysis, it was determined that the mesh configuration comprising 297,680 cells emerged as the optimal choice for conducting the primary simulations in this study. By ensuring an appropriate mesh density and structure, this selection of cell count

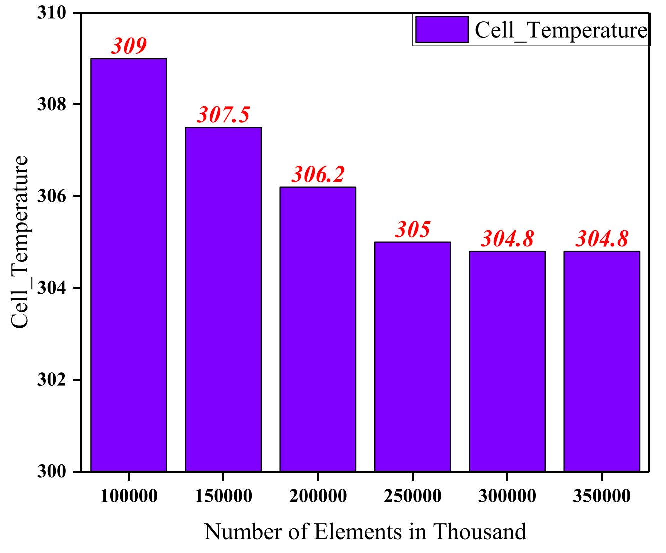

FIGURE 3 Cell temperature and element count.

strikes a harmonious balance between computational efficiency and the accuracy of temperature predictions essential for the battery pack analysis.

2.3 | Modeling: Multiscale multidomain (MSMD) (Newman, Tiedemann, Gu, and Kim [NTGK]) battery model

A full three-dimensional model that integrates battery chemistry and physics is necessary for accurate thermal analysis of battery systems. This makes tracing the battery's interior heat flow and thermal resistance easier. Lithium-ion transport works at the atomic level. Nevertheless, temperature distribution at the cell length scale is the main focus of battery thermal study. Using individual domains for numerical analyses of complicated cells is computationally demanding. Therefore, the current simulation uses the NTGK model, a targeted submodel, within the MSMD framework to simulate accurately yet economically. An empirical voltage versus current equation and an energy-saving equation for heat generation are included in the NTGK model.[20]

$$\nabla \cdot \vec{i}_{\mathrm{e}} = j. \tag{1}$$

The symbol $\vec{i}_{\mathrm{e}}$ represents the linear current density at the electrode interface in a battery system. Here, “e” specifies the electrode under consideration. This notation is especially helpful when examining multielectrode systems, where each electrode may have unique characteristics or behaviors. Conversely, “j” stands for the current density required in the battery to transfer charge carriers between the positive and negative electrodes. Understanding the flow of electrical charge within the battery throughout charging and discharging cycles depends on this current density. It considers the flow of ions or electrons between the two electrodes via the electrolyte or active material. “1_{s}” and “j” essentially support battery system analysis. “1_{s}” concentrates on the current density, however.

The expression for ohm's law, which controls the electrode, is:[20]

$$\vec{i}_e = \nabla \sigma_e \phi_e. \tag{2}$$

The electrode conductivity (σ_e) and the electrode potential (ϕ_e) are introduced in Equation (2) and are essential to understanding the electrochemical behavior at the electrode interface.

By integrating Equations (1) and (2), a fundamental relationship between electrode voltage and current density is produced. The result of this combination is Equation (3), which contains the current control equations for the positive and negative electrodes and is crucial to comprehending the electrochemical dynamics of the battery system as a whole[20]

$$\nabla \cdot (\sigma_+ \nabla \phi_+) = -\nabla \cdot (\sigma_- \nabla \phi_-) = j, \tag{3}$$

$$\text{where } j = j_{ECh} - j_{short}.$$

The subscripts + and − are used in Equation (3) to indicate which electrode is positive and which is negative. The values ϕ_+ and ϕ_- represent the phase potentials, and the parameters σ_+ and σ_- represent each electrode's effective conductivity. Moreover, j_{ECh} indicates the volumetric current density, whereas "j_{short}" represents the current density coming from a short circuit.

Newman and Tiedemann improved this further by adding semiempirical parameters U and Y and accounting for electrode polarization. Improving the link between voltage and current in Equation (3) enhanced the model's capacity to represent the complex electrochemical dynamics at the electrodes. Equation (4) showcases the enhanced association between voltage and volumetric current density, which indicates progress in modeling precision and comprehension of electrochemical events.[20]

$$j_{ECh} = \frac{1}{Vol_b} Y [U - (\varphi_+ - \varphi_-)]. \tag{4}$$

The battery volume is represented by Vol_b in Equation (4), and the semiempirical parameters U and Y, which connect the thermal and electrical characteristics of LIBs, are unique to the NTGK model. With U standing for equilibrium voltage and Y for conductance, U and Y reflect the battery's voltage and internal resistance during charge and discharge dynamics. Originally, iterative trial and error was used to determine U and Y. The NTGK method suggested that the polynomial fitting of charge and discharge curves for discharge tests at different rates be used in place of this procedure.

It is stated as follows how U, Y, and DoD have enhanced functional correlation.[20]

$$U = \left[\sum_{n=0}^{5} a_n (DoD)^n\right] - C_2 (T - T_{ref}), \tag{5}$$

$$Y = \left[\sum_{n=0}^{5} b_n (DoD)^n\right] \times \exp\left[-C_1 \left(\frac{1}{T} - \frac{1}{T_{ref}}\right)\right], \tag{6}$$

$$DoD = \frac{Vol_b}{3600Q_b}\int_0^t j\,dt, \tag{7}$$

where T is the typical temperature of the battery and T_{ref} is the reference temperature in Equations (5)–(7). The correction constants C_1 and C_2, which have respective values of 1800 and −0.000958, are utilized. The symbols Vol_b, and Q_b denote the battery capacity and volume, respectively. Equations (5) and (6)'s coefficients a_n and b_n were found by discharging tests carried out at various speeds. Battery voltage, conductance, and U, Y do not directly correlate functionally; one must compute the relationship by transformation.

The following formula is used to determine energy conservation in LIBs.[20]

$$\frac{\partial p_b C_{p_b} T}{\partial t} = \nabla(k_b \nabla T) + q_{gen}. \tag{8}$$

Several parameters are introduced in Equation (8): T is the average cell temperature, k_b is thermal conductivity, q_{gen} is the overall rate of heat production within the cell, and p_b is cell density. C_{p_b} is cell-specific heat capacity. The components of the NTGK model that contribute to the overall cell heat production rate q_{gen} are listed in Equation (9).[20]

$$q_{gen} = [q_{irr} + q_{rev}] + \left[\sigma_+ \nabla\phi_+^2 + \sigma_- \nabla\phi_-^2\right] + q_{short}. \tag{9}$$

Equation (9) shows the first term represents the electrochemical process of heat.$[q_{irr} + q_{rev}]$ and the ohmic heat is represented by second-term $\left[\sigma_+ \nabla\phi_+^2 + \sigma_- \nabla\phi_-^2\right]$. Heat resulting from a short circuit is also taken into consideration by the third term,q_{short}. Specifically, in the first term $[q_{irr} + q_{rev}]$, q_{irr} represents the irreversible heat resulting from over-potential, and q_{rev} represents the reversible heat resulting from entropy changes.[20]

$$q_{irr} = j\,[V_{oc} - (\phi_+ - \phi_-)], \tag{10}$$

$$q_{rev} = -jT\frac{dV_{oc}}{dT}. \tag{11}$$

Understanding the behavior of batteries requires understanding the open-circuit voltage, or Voc. The number of moles (n) engaged in the lithium-ion incorporating reaction and the entropy change (VS) are related to the derivative of V_{oc}, concerning battery temperature. This relationship captures the complex interactions in the battery system between temperature, entropy, and chemical reactions.[20]

$$\frac{dV_{oc}}{dT} = \frac{\triangle S}{n}. \tag{12}$$

The provided equation for determining the thermophysical characteristics of MXene enhanced with dielectric fluids is outlined as follows.[19]

$$\rho_{\mathrm{ndf}} = (1-\varphi)\rho_{\mathrm{df}} + \varphi\rho_{\mathrm{np}}, \tag{13}$$

$$(\rho C)_{\mathrm{ndf}} = (1-\varphi)(\rho C)_{\mathrm{df}} + \varphi(\rho C)_{\mathrm{np}}, \tag{14}$$

$$k_{\mathrm{ndf}} = \left(\frac{k_{\mathrm{np}} + 2k_{\mathrm{df}} - 2(k_{\mathrm{df}} - k_{\mathrm{np}})\varphi}{k_{\mathrm{np}} + 2k_{\mathrm{df}} + 2(k_{\mathrm{df}} - k_{\mathrm{np}})\varphi}\right)k_{\mathrm{df}}. \tag{15}$$

Mass conservation equation, momentum conservation equations, and turbulent kinetic energy and dissipation rate equation as follows.[19]

$$\frac{\partial \rho}{\partial t} + \mathrm{div}(\rho u) = 0, \tag{16}$$

$$\frac{\partial(\rho u)}{\partial t} + \mathrm{div}(\rho u\mathbf{u}) = -\frac{\partial p}{\partial x} + \mathrm{div}(\mu \mathrm{grad}\, u) + \left[-\frac{\partial(\rho \overline{u'^2})}{\partial x} - \frac{\partial(\rho \overline{u'v'})}{\partial y} - \frac{\partial(\rho \overline{u'w'})}{\partial z}\right], \tag{17}$$

$$\frac{\partial(\rho v)}{\partial t} + \mathrm{div}(\rho v\mathbf{u}) = -\frac{\partial p}{\partial y} + \mathrm{div}(\mu \mathrm{grad}\, v) + \left[-\frac{\partial(\rho \overline{v'u'})}{\partial x} - \frac{\partial(\rho \overline{v'^2})}{\partial y} - \frac{\partial(\rho \overline{v'w'})}{\partial z}\right], \tag{18}$$

$$\frac{\partial(\rho w)}{\partial t} + \mathrm{div}(\rho w\mathbf{u}) = -\frac{\partial p}{\partial z} + \mathrm{div}(\mu \mathrm{grad}\, w) + \left[-\frac{\partial(\rho \overline{w'u'})}{\partial x} - \frac{\partial(\rho \overline{w'v'})}{\partial y} - \frac{\partial(\rho \overline{w'^2})}{\partial z}\right], \tag{19}$$

$$\frac{\partial(\rho E)}{\partial t} + \mathrm{div}(\rho E\mathbf{u}) = \mathrm{div}(k \mathrm{grad}\, T) + \left[-\frac{\partial(\rho \overline{u'E'})}{\partial x} - \frac{\partial(\rho \overline{v'E'})}{\partial y} - \frac{\partial(\rho \overline{w'E'})}{\partial z}\right], \tag{20}$$

$$\frac{\partial}{\partial t}(\rho k) + \frac{\partial}{\partial x_i}[\rho k u_i] = \frac{\partial}{\partial x_j}\left[\alpha_{\mathrm{k}}\mu_{\mathrm{eff}}\frac{\partial k}{\partial x_j}\right] + G_{\mathrm{k}} + G_{\mathrm{b}} - \rho\varepsilon + S_{\mathrm{k}}. \tag{21}$$

The Reynolds number formula for pipe flow[19]

$$Re = \frac{\rho_{\mathrm{f}} \cdot v_{\mathrm{f}} \cdot D_{\mathrm{hy}}}{\mu_{\mathrm{f}}}, \tag{22}$$

where D_{hy} is the hydraulic diameter.

The transient analysis features a pressure-based solver with a constant convective heat transfer coefficient on the battery pack's outer surface. Starting at 300 K and 1 bar in standard atmospheric conditions, the dielectric fluid velocity varies iteratively to optimize the BTMS, aiming for peak performance. This dynamic approach allows for fine-tuning the cooling process to achieve an optimal outcome for the system.

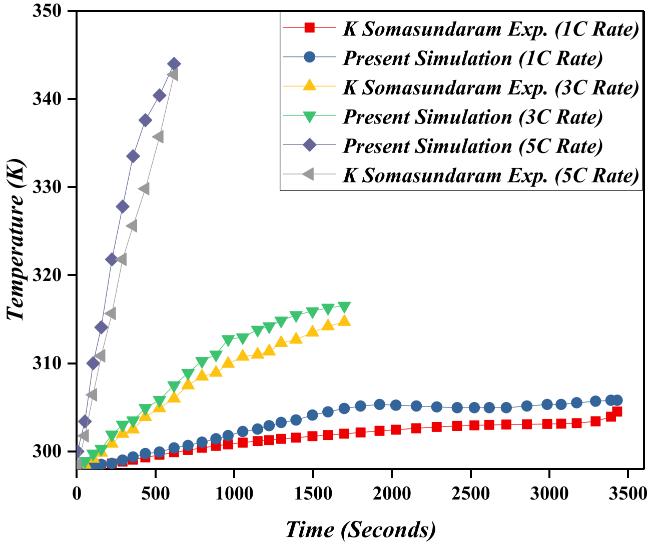

FIGURE 4 Model validation (temperature vs. time).

2.4 | Top of form

2.4.1 | Validation and verification of data

Model validation is integral in battery thermal management research. Validation with Somasundaram et al.[21] data across discharge rates (1C, 2C, 5C) reveals close agreement, with differences below 5%. C-rate in LIBs refers to the rate at which a battery's capacity is charged or discharged over a specific timeframe. Graphical representations visually highlight data comparisons, aiding swift identification of similarities and disparities between simulation and actual results, bolstering confidence in model accuracy. The validation process in this research demonstrates the accuracy and reliability of the simulation model in capturing complex thermal behavior in LIB systems at varying discharge rates, as shown in Figure 4.

Close alignment between experimental data and simulation outcomes enhances the model's credibility, supporting informed decisions on system design and optimization. Effective validation gives researchers confidence in the model's predictive capabilities, offering a robust tool for system performance analysis and optimization in BTMSs. This validation process advances BTMS research and underscores the model's applicability for practical implementations, contributing significantly to the field's progress.

3 | RESULT AND DISCUSSION

3.1 | Effect of cell temperature contour without immersion cooling at 5C-rates

The image represents in Figure 5, a thermal analysis of two batteries connected in series with a busbar, undergoing a discharge at a 5C-rate using an MSMD battery model. The batteries are discharged at a 5C-rate, five times their rated capacity per hour. The maximum and minimum

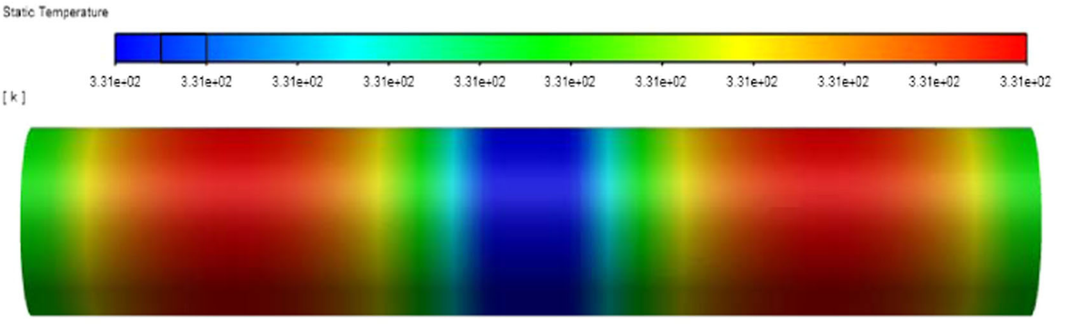

FIGURE 5 Impact of cell temperature on 5C-rates without immersion cooling.

cut-off voltages are set at 4.2 and 3.7 V, respectively, with a nominal voltage of 4V. Each battery has a capacity of 4.2 mAh, and the discharge current is 1 A. During the discharge process, the maximum surface temperature of the batteries reaches 331.4 K, significantly higher than the reference temperature of 300 K.

This thermal map is crucial for understanding the heat distribution and potential hotspots that may arise during high-rate discharges, informing strategies for thermal management and safety in battery design. The color-coded gradient visually communicates the temperature variation across the battery surfaces, emphasizing the need for effective cooling systems in high-performance applications. The precise control of discharge rates, voltage thresholds, and temperature monitoring is essential for optimizing battery life and performance.

3.2 | Effect of cell temperature at 5C discharge rate immersed in flowing dielectric fluid

Cell temperature management is critical in a 5C discharge rate scenario, especially when using different dielectric fluids as coolants, as shown in Figure 6. At a specific flow velocity of 0.01 m/s, four dielectric fluids—ester oil, mineral oil, kerosene oil, and Novec 7200—were evaluated for their effectiveness in managing the cell temperature of LIBs. Among these, ester oil demonstrated superior performance as a cooling fluid. Without any dielectric fluid, the cell temperature rapidly rises to 331 K, significantly exceeding the safe operating conditions for LIBs. This elevated temperature can lead to performance degradation, reduced cycle life, and increased safety risks due to potential thermal runaway. As such, efficient thermal management is essential to maintain optimal performance and longevity of battery cells.

When comparing the effectiveness of the four dielectric fluids, ester oil emerged as the most efficient, maintaining the cell temperature at 305.84 K. In contrast, kerosene oil kept the temperature at 306.14 K, mineral oil at 306.5 K, and Novec 7200 at 306 K. These findings indicate that these fluids can substantially reduce the cell temperature compared with the scenario without any coolant. Specifically, ester oil achieved a 44% reduction in cell temperature, and kerosene oil reduced it by 42.86%, mineral oil by 42.51%, and Novec 7200 by 43.11%. During the initial 150 s of the discharge process, all fluids performed similarly, maintaining nearly constant temperatures. This consistency indicates their initial effectiveness in managing the thermal load. However, beyond this period, the performance of the fluids began to diverge.

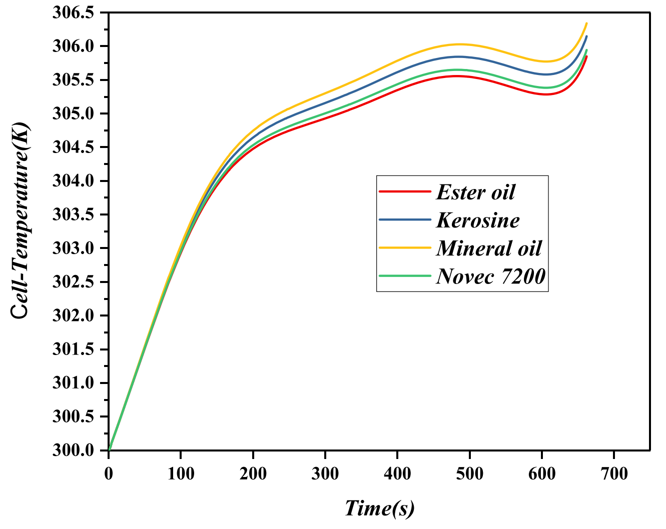

FIGURE 6 Impact of a cell submerged in a flowing dielectric fluid at 5C-rates of discharge.

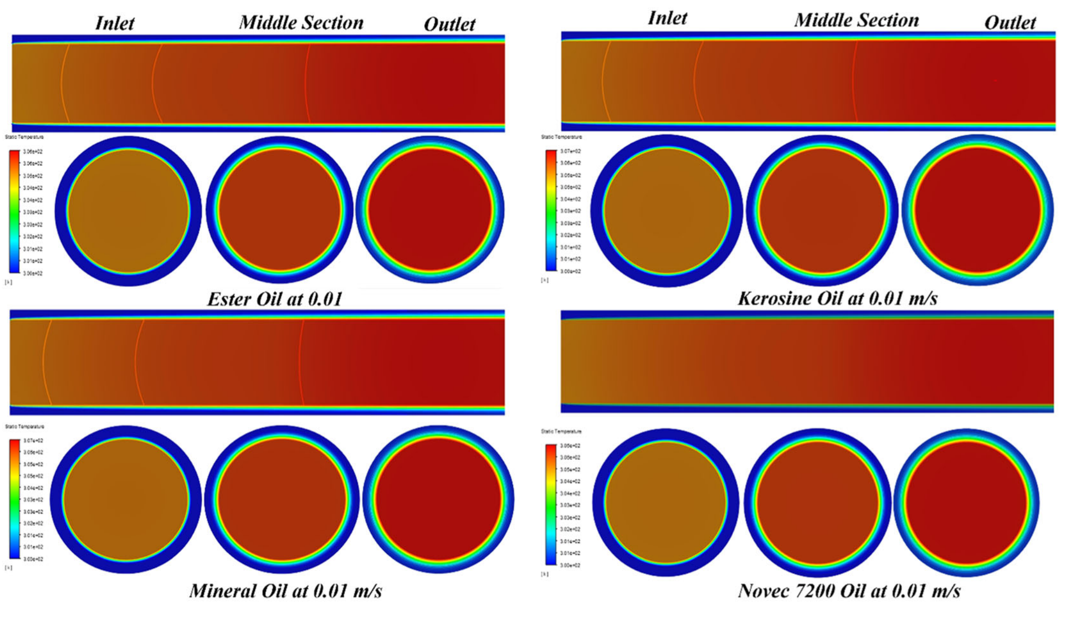

FIGURE 7 Temperature contours for cells submerged in flowing dielectric fluids.

Ester oil managed the thermal energy effectively even after 150 s, highlighting its robustness in prolonged high-rate discharge conditions. The slight edge of ester oil can be attributed to its higher specific heat capacity and thermal conductivity, which enable it to absorb and dissipate more heat from the cell more effectively.

The temperature contours for the inlet, middle, and outlet sections of the cylindrical battery thermal system in kerosene oil, mineral oil, and Novec 7200 have been presented in Figure 7.

On the other hand, kerosene oil, mineral oil, and Novec 7200, all-dielectric fluids, started showing signs of decreased performance over time despite their initial effectiveness. This decline is likely due to their comparatively lower thermal conductivity and specific heat capacity, limiting their continuous ability to manage increased thermal energy. Given these findings, it is clear that selecting the right cooling fluid is crucial for designing efficient BTMSs, particularly for applications involving rapid discharge rates, such as EVs or high-demand energy storage systems. Among the fluids tested, ester oil is optimal for sustaining battery health under extreme operational conditions. Its superior thermal performance ensures that the battery cells operate within safe temperature ranges, enhancing the battery systems' reliability, safety, and longevity.

3.3 | Effect of cell temperature at 5C discharge for MXene-based ester oil at different velocities

In BTMSs, particularly for high-rate discharge scenarios such as the 5C discharge rate, it is crucial to maintain optimal cell temperatures to ensure safety, performance, and longevity. In one such study examining the effectiveness of battery cooling using flowing dielectrics, ester oil mixed with MXene, a family of compounds known for their high thermal and electrical conductivity, was evaluated at different flow velocities to gauge its cooling capabilities. Under normal conditions without active or passive thermal management, the cell temperature can soar up to a critical 58.1°C (331.1 K) during a 5C discharge. This temperature level not only jeopardizes the safety of the battery cells by increasing the risk of thermal runaway but can also sharply diminish their performance and cycle life. However, introducing a flowing ester oil and MXene mixture as a cooling medium can drastically mitigate these temperature rises.

Variations in cell temperature at a 5C discharge rate submerged in MXene-based ester oil dielectric fluid at varying flow velocity and time are presented in Figure 8. The results from Figure 8 revealed that even at a slow flow velocity of 0.01 m/s, the ester oil mixture reduces the

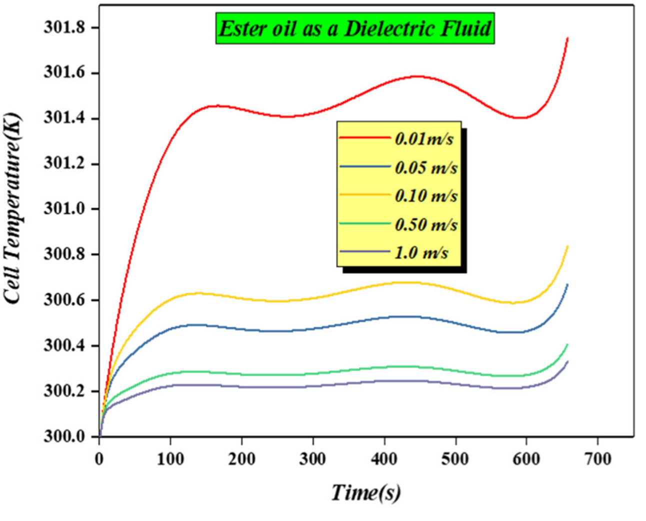

FIGURE 8 Cell temperature for MXene-based dielectric fluid at varying flow velocity.

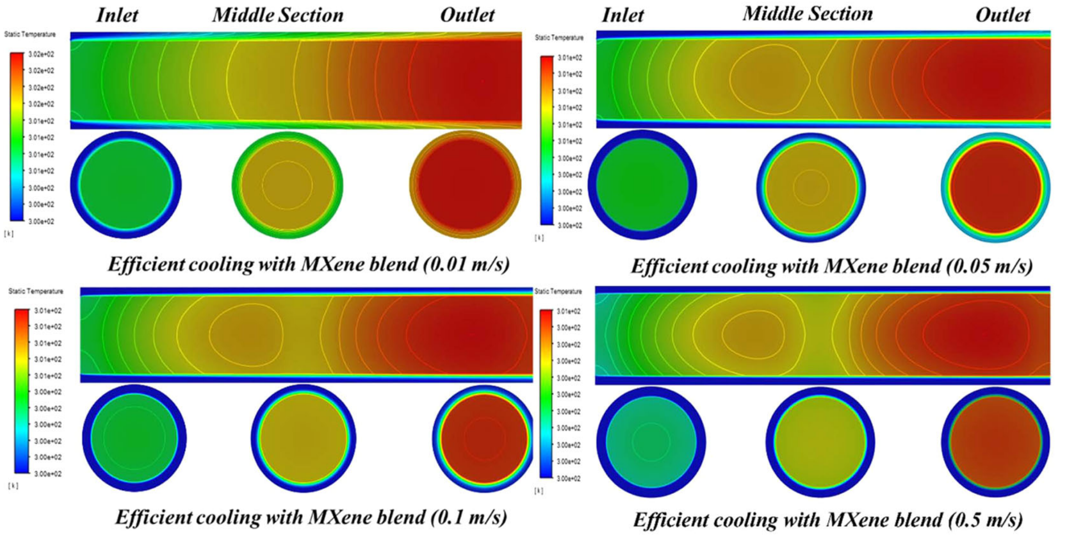

FIGURE 9 Cell temperature contour for MXene-based dielectric fluid at varying flow velocity.

cell temperature by an impressive 50%, highlighting the immediate impact of introducing a fluid dynamic cooling process. As the flow velocity increases, the cooling effect becomes more pronounced: at 0.05 and 0.1 m/s, the temperature reductions reach 51.89% and 52.155%, respectively. At higher velocities of 0.5 and 1 m/s, the cutbacks in temperature climb further to 52.58% and 54%. The enhanced heat transfer at increased fluid velocities can be attributed to improved mixing and more significant surface contact between the cooling fluid and the battery cells, facilitating more effective heat dissipation. MXene's incorporation into the ester oil significantly contributes to this performance because of its high thermal conductivity, which aids in spreading the heat more uniformly and quickly away from the cells.

This data underscores the potential of combining advanced materials like MXene with traditional cooling methods to create highly efficient thermal management strategies for high-discharge-rate LIBs. The temperature contours for the inlet, middle, and outlet sections of the cylindrical battery thermal system in MXene-based ester oil dielectric fluid have been presented in Figure 9. Employing such fluid dynamic solutions could be particularly critical in EVs and high-performance electronic devices, where managing extreme heat is paramount for safety and efficiency.

3.4 | Effect on the dielectric fluid temperature at a 5C discharge rate

In a BTMS, the dielectric fluid plays a crucial role in dissipating heat generated during the battery discharge process, helping to maintain optimal operating temperatures. When evaluating the effect of different dielectric fluids—ester oil, kerosene oil, mineral oil, and Novec 7200—flowing over a series-connected cylindrical tube battery at a velocity of 0.01 m/s during a 5C discharge rate, the temperature of the fluids becomes a critical factor as presented in Figure 10. These dielectric fluids absorb the heat generated by the cells as the batteries discharge, raising the fluid's temperature. It was found that during this operation, ester oil had the

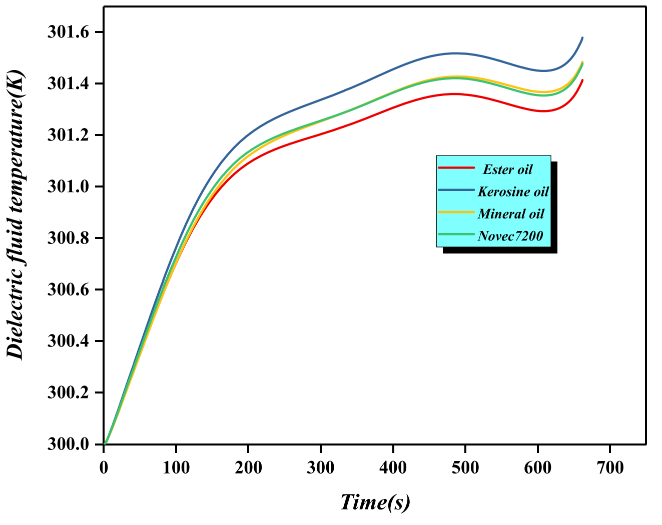

FIGURE 10 Effect on the dielectric fluid temperature at a 5C discharge rate.

lowest mass-average fluid temperature, followed by Novec 7200, mineral oil, and kerosene oil, in that order. This ranking indicates the varying effectiveness of these fluids in absorbing and dissipating heat from the battery cells during high-rate discharges.

Ester oil dielectric fluid stands out with the lowest mass-average fluid temperature, suggesting that it is the most efficient coolant among the tested options for immersion cooling. The ability of ester oil to maintain a lower average temperature compared with the other fluids indicates its superior thermal conductivity and specific heat capacity, enabling it to efficiently absorb and dissipate heat, thereby effectively cooling the battery cells during the discharge process. On the other hand, lower-performing fluids like kerosene oil and mineral oil exhibit higher mass-average temperatures, indicating that they are less efficient in managing the heat generated by the battery cells. This reduced cooling capability could lead to increased temperatures within the battery system, potentially compromising performance, cycle life, and overall reliability. The findings highlight the crucial role of the dielectric fluid in BTMSs, emphasizing the importance of selecting the most suitable coolant for maintaining optimal operating temperatures and enhancing the overall efficiency and safety of battery systems, particularly in high-demand applications, like, EVs and energy storage systems.

3.5 | Variation of voltage with and without immersion cooling

In BTMSs focusing on voltage variations with and without immersion cooling, the simulation evaluates the impact of dielectric fluids like ester oil, kerosene oil, mineral oil, and Novec 7200 on reducing voltage drop during discharge. The scenario from Figure 11 involves a battery with a minimum stop voltage of 3 V, a maximum stop voltage of 4.2 V, and a nominal voltage of 4 V. The simulation results show a significant duration difference between immersion cooling with dielectric fluids and scenarios without cooling. With immersion cooling, the voltage drop occurs in about 661 s, whereas without such cooling measures, the voltage drop takes approximately 680 s. The observed difference in the time taken for the voltage drop in the two

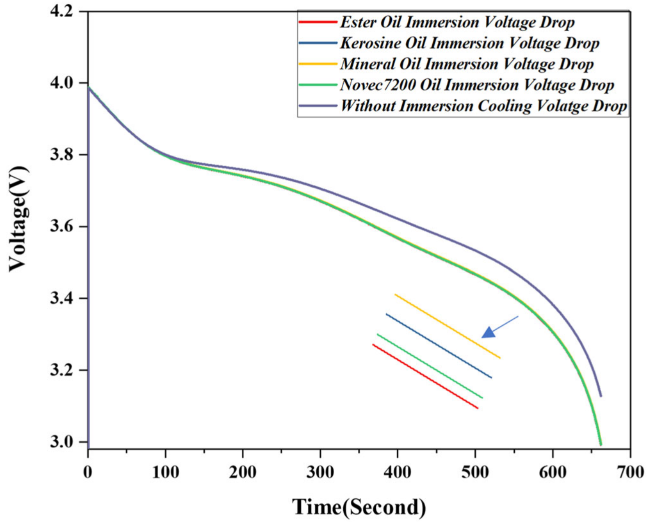

FIGURE 11 Voltage variation for immersed and nonimmersed battery pack with time.

scenarios can be attributed to the influence of effective thermal management provided by the dielectric fluids. When the battery operates without any cooling mechanisms, heat generated during discharge accumulates within the battery cells, leading to a more rapid voltage drop due to increased internal resistance and inefficiencies in energy transfer. As a result, the battery reaches the minimum stop voltage sooner, indicating a reduced usable capacity.

Conversely, when the battery is immersed in dielectric fluids like ester oil, kerosene oil, mineral oil, or Novec 7200, these fluids efficiently absorb and dissipate heat, maintaining optimal operating temperatures within the battery cells. This enhanced thermal management reduces the voltage drop by preventing the cells from overheating and maintaining more stable internal conditions. The temperature regulation provided by the cooling fluids helps preserve the cells' performance, cycle life, and overall efficiency before reaching the minimum stop voltage. In essence, the utilization of dielectric fluids in immersion cooling significantly enhances the thermal characteristics of the battery, resulting in a more gradual voltage drop over time. The ability of these fluids to manage heat effectively extends the battery's operational capacity and safeguards against potentially detrimental effects associated with rapid discharges, ultimately contributing to improved performance and safety within battery systems. This difference in seconds between the cooling and noncooling scenarios underscores the critical role of thermal management strategies in optimizing battery performance and longevity in high-demand applications, like, EVs and energy storage systems.

4 | CONCLUSION

In this work, a unique cylindrical shell with Li-ion cell cooling is assessed, analyzing temperatures and voltage drops under various fluid velocities, using active and MXene-nanoenhanced ester oil dielectric fluids at 5C discharge rates. The main conclusions of the study are listed below.

- The temperature of the dielectric fluid drops as the velocity of the fluid gets higher. Ester oil went up to 300.029 K with 1% v/v MXene nanoparticle when it was discharged at 1 m/s and 5C.
- Higher cell discharge rates cause the temperature of the battery system's cells to progressively increase. At a C-rate of 5C, the cell temperature reached its lowest point of 300.33 K at 1 m/s, while for MXene-based ester oil dielectric fluid reached its highest point at 301.77 K at 0.01 m/s.
- Compared with other fluids, MXene-based ester oil dielectric fluid reduces cell temperature by half at constant C-rates and velocities of 0.01 m/s.
- When compared with immersion cooling, the discharge duration at constant 5C-rates is 19 s longer without cooling, despite the fact that the voltage drop is reducing.
- The ester oil infused with MXene nanoparticle exhibits exceptional cooling capabilities, maintaining reduced temperatures even at elevated discharge rates and possibly achieving a 50% temperature decrease at reduced speeds.

The above findings emphasize the importance of maintaining ideal cell temperatures for both safety and performance, which provide crucial insights for advancing battery cooling systems in high-demand applications such as energy storage devices and electric cars to improve battery performance. The limitation of this study is the entire simulation is based on single-phase analysis, and it is recommended to do two-phase analysis for further study as two-phase analysis, involving nanoparticles and base fluids separately, enhances simulation accuracy by considering interactions between particles and fluid.

NOMENCLATURE

b	busbar
C_p	specific heat
D_{hy}	hydraulic diameter
DoD	depth of discharge
$\vec{i}_{\text{e}}$	current density at the electrode
j	current density
j_{ECh}	density of volumetric current
k_{b}	thermal conductivity
q_{gen}	rate at which the battery produces heat overall
q_{irr}	over potential causes irreversible heat
q_{rev}	reversible heat due to entropy change
q_{short}	heat produced by the circuit break
Re	Reynolds number
T	average battery temperature
T_{ref}	reference temperature
U	parameters of the NTGK model
v_{f}	velocity of fluid
V_{oc}	open circuit voltage
Vol_{b}	battery capacity
Y	model parameters for the NTGK

GREEK SYMBOLS

μ_{f}	dynamic viscosity
ϕ_+	phase potential of the positive electrode
ϕ_-	phase potential of the negative electrode

ϕ_e potential of electrodes
φ_+ phase potential of the positive electrode
φ_- phase potential of the negative electrode
ρ density
σ_e conductivity of the electrodes

SUBSCRIPTS

df dielectric fluid
ndf nanoenhanced dielectric fluid
np nanoparticle
oc open circuit
ref reference

CONFLICT OF INTEREST STATEMENT

The authors declare no conflict of interest.

DATA AVAILABILITY STATEMENT

The data that support the findings of this study are available from the corresponding author upon reasonable request.

ORCID

Rashmi Rekha Sahoo https://orcid.org/0000-0003-3133-6626

REFERENCES

1. Wu W, Wang S, Wu W, Chen K, Hong S, Lai Y. A critical review of battery thermal performance and liquid based battery thermal management. *Energy Convers Manage*. 2019;182:262-281.
2. Fayaz H, Afzal A, Samee ADM, et al. Optimization of thermal and structural design in lithium-ion batteries to obtain energy efficient battery thermal management system (BTMS): a critical review. *Arch Comput Methods Eng*. 2022;29(1):129-194.
3. Wang Q, Jiang B, Li B, Yan Y. A critical review of thermal management models and solutions of lithium-ion batteries for the development of pure electric vehicles. *Renewable Sustainable Energy Rev*. 2016;64:106-128.
4. Kumar R, Goel V. A study on thermal management system of lithium-ion batteries for electrical vehicles: a critical review. *J Energy Storage*. 2023;71:108025.
5. Kim J, Oh J, Lee H. Review on battery thermal management system for electric vehicles. *Appl Therm Eng*. 2019;149:192-212.
6. Wang M, Teng S, Xi H, Li Y. Cooling performance optimization of air-cooled battery thermal management system. *Appl Therm Eng*. 2021;195:117242.
7. Chen K, Wu W, Yuan F, Chen L, Wang S. Cooling efficiency improvement of air-cooled battery thermal management system through designing the flow pattern. *Energy*. 2019;167:781-790.
8. Wang C, Xi H, Wang M. Investigation on forced air-cooling strategy of battery thermal management system considering the inconsistency of battery cells. *Appl Therm Eng*. 2022;214:118841.
9. Chen K, Zhang Z, Wu B, Song M, Wu X. An air-cooled system with a control strategy for efficient battery thermal management. *Appl Therm Eng*. 2024;236:121578.
10. Akbarzadeh M, Kalogiannis T, Jaguemont J, et al. A comparative study between air cooling and liquid cooling thermal management systems for a high-energy lithium-ion battery module. *Appl Therm Eng*. 2021;198:117503.

11. Yang W, Zhou F, Zhou H, Wang Q, Kong J. Thermal performance of cylindrical lithium-ion battery thermal management system integrated with mini-channel liquid cooling and air cooling. *Appl Therm Eng*. 2020;175:115331.
12. Chen K, Chen Y, Li Z, Yuan F, Wang S. Design of the cell spacings of battery pack in parallel air-cooled battery thermal management system. *Int J Heat Mass Transfer*. 2018;127:393-401.
13. Wang H, Tao T, Xu J, Mei X, Liu X, Gou P. Cooling capacity of a novel modular liquid-cooled battery thermal management system for cylindrical lithium-ion batteries. *Appl Therm Eng*. 2020;178:115591.
14. Zou Z, Xie J, Luo Y, Zhang G, Yang X. Numerical study on a novel thermal management system coupling immersion cooling with cooling tubes for power battery modules. *J Energy Storage*. 2024;83:110634.
15. Satyanarayana G, Ruben Sudhakar D, Muthya Goud V, Ramesh J, Pathanjali GA. Experimental investigation and comparative analysis of immersion cooling of lithium-ion batteries using mineral and therminol oil. *Appl Therm Eng*. 2023;225:120187.
16. Jithin KV, Rajesh PK. Numerical analysis of single-phase liquid immersion cooling for lithium-ion battery thermal management using different dielectric fluids. *Int J Heat Mass Transfer*. 2022;188:122608.
17. Hemavathi S, Thiru Kumaran A, Srinivas S, Prakash AS. Synthetic ester-based forced flow immersion cooling technique for fast discharging lithium-ion battery packs. *J Energy Storage*. 2024;97:112852.
18. Qi W, Huang W, Niu J, Chen F, Chen B, Chen Y. Thermal management of power battery based on flexible Swiss roll type liquid cooling micro-channel. *Appl Therm Eng*. 2023;219:119491.
19. Gaur SK, Sahoo RR, Sarkar J. Numerical investigation on thermohydraulic and exergy performance enhancement for triplex concentric tube heat exchanger using MXene nanofluids. *Int J Energy Water Resour*. 2024;8:1-16.
20. Kumari P, Paswan M. Thermal management system of battery using nano-coolant. In: Mishra A, Gupta D, Chety G, eds. *International Conference on Advances in IoT and Security with AI*. Springer Nature Singapore; 2023:173-181.
21. Somasundaram K, Birgersson E, Mujumdar AS. Thermal–electrochemical model for passive thermal management of a spiral-wound lithium-ion battery. *J Power Sources*. 2012;203:84-96.
22. Zhang J, Shao D, Jiang L, et al. Advanced thermal management system driven by phase change materials for power lithium-ion batteries: a review. *Renewable Sustainable Energy Rev*. 2022;159:112207.
23. Weng J, Xiao C, Yang X, et al. An energy-saving battery thermal management strategy coupling tubular phase-change-material with dynamic liquid cooling under different ambient temperatures. *Renewable Energy*. 2022;195:918-930.
24. Luo M, Zhang Y, Wang Z, et al. Thermal performance enhancement with snowflake fins and liquid cooling in PCM-based battery thermal management system at high ambient temperature and high discharge rate. *J Energy Storage*. 2024;90:111754.
25. Shojaeefard MH, Molaeimanesh GR, Ranjbaran YS. Improving the performance of a passive battery thermal management system based on PCM using lateral fins. *Heat and Mass Transfer*. 2019;55:1753-1767.
26. Pu J, Li Y, Li RC, et al. Design and Performance of a Compact Lightweight Hybrid Thermal Management System Using Phase Change Material and Liquid Cooling with a Honeycomb-like Structure for Prismatic Lithium-ion Batteries. 2024. Available at SSRN 4931222.
27. Chen J, Kollmeyer P, Panchal S, Masoudi Y, Gross O, Emadi A. eds. Experimental results of battery power capability measurement on cells with different state of health levels. In: *2024 IEEE Transportation Electrification Conference and Expo (ITEC)*; 2024:1-6.
28. Tran MK, DaCosta A, Mevawalla A, Panchal S, Fowler M. Comparative study of equivalent circuit models performance in four common lithium-ion batteries: LFP, NMC, LMO, NCA. *Batteries*. 2021;7(3):51.
29. Bais AR, Subhedar D, Panchal S. Experimental Investigations of a Novel Phase Change Material and Nano Enhanced Phase Change Material Based Passive Battery Thermal Management System for Li-ion Battery Discharged at a High C Rate. 2024. Available at SSRN 4743339.
30. Nagaraja S, Nagegowda KU, Kumar V A, et al. Influence of the fly ash material inoculants on the tensile and impact characteristics of the aluminum AA 5083/7.5 SiC composites. *Materials*. 2021;14:2452.
31. Suryavanshi SS, Ghanegaonkar PM, Panchal S. *Enhancing Efficiency in Air-cooled Cylindrical Battery Temperature Management Systems for Electric Vehicles: A CFD Analysis of a Novel Uniform Flow Distribution Plate*. 2024. Available at SSRN: https://ssrn.com/abstract=4888691

32. Pu JH, Ping X-F, Panchal S, et al. Structural Optimization of a Serpentine-channel Cold Plate for Thermal Management of Lithium-ion Battery Based on the Field Synergy Principle. 2024. Available at SSRN 4795285.
33. Talele V, Moralı U, Najafi Khaboshan H, et al. Improving battery safety by utilizing composite phase change material to delay the occurrence of thermal runaway event. *Int Commun Heat Mass Transfer*. 2024;155:107527.
34. Jiaqiang E, Xiao H, Tian S, Huang Y. A comprehensive review on thermal runaway model of a lithium-ion battery: mechanism, thermal, mechanical, propagation, gas venting and combustion. *Renewable Energy*. 2024;229:120762.
35. Xiao H, E J, Tian S, Huang Y, Song X. Effect of composite cooling strategy including phase change material and liquid cooling on the thermal safety performance of a lithium-ion battery pack under thermal runaway propagation. *Energy*. 2024;295:131093.
36. Shengxin E, Cui Y, Liu Y, Yin H. Effects of the different phase change materials on heat dissipation performances of the ternary polymer Li-ion battery pack in hot climate. *Energy*. 2023;282:128805.
37. Liu Y, Cui Y, Wu A, Yin H. Corrigendum to "Effects of composite cooling strategy including phase change material and cooling air on the heat dissipation performance improvement of lithium-ion power batteries pack in hot climate and its catastrophe evaluation" [Energy 283 (2023) 129074]. *Energy*. 2023;284:129311.
38. Jiaqiang E, Qin Y, Zhang B, Yin H, Tan Y. Effects of heating film and phase change material on preheating performance of the lithium-ion battery pack with large capacity under low temperature environment. *Energy*. 2023;284:129280.
39. Ma Y, Yang H, Zuo H, et al. Three-dimensional EG@ MOF matrix composite phase change materials for high efficiency battery cooling. *Energy*. 2023;278:127798.
40. Ma Y, Yang H, Zuo H, et al. EG@ Bi-MOF derived porous carbon/lauric acid composite phase change materials for thermal management of batteries. *Energy*. 2023;272:127180.
41. Ma Y, Wei R, Zuo H, et al. Development of hierarchical MOF-based composite phase change materials with enhanced latent heat storage for low-temperature battery thermal optimization. *Energy*. 2023;283:129001.
42. Ma Y, Wei R, Zuo H, et al. N-doped EG@ MOFs derived porous carbon composite phase change materials for thermal optimization of Li-ion batteries at low temperature. *Energy*. 2024;286:129637.
43. Yi F, E J, Zhang B, et al. Effects analysis on heat dissipation characteristics of lithium-ion battery thermal management system under the synergism of phase change material and liquid cooling method. *Renewable Energy*. 2022;181:472-489.
44. Verma A, Saikia T, Saikia P, Rakshit D, Ugalde-Loo CE. Thermal performance analysis and experimental verification of lithium-ion batteries for electric vehicle applications through optimized inclined mini-channels. *Appl Energy*. 2023;335:120743.

How to cite this article: Singh NK, Sahoo RR. Performance enhancement for a novel cylindrical system Li-ion battery with MXene-based dielectric fluid for immersion cooling. *Heat Transfer*. 2025;54:1093-1115. doi:10.1002/htj.23208